



ORIGINAL ARTICLE

Antibacterial and antioxidant screening applications of reduced-graphene oxide modified ternary SnO₂-NiO-CuO nanocomposites



Sirajul Haq^{a,*}, Maria Rashid^a, Farid Mena^{b,*}, Nadia Shahzad^c,
Muhammad Imran Shahzad^d, Sulaiman Y.M. Alfaifi^e, O. Madkhali^f,
Mahmood D. Aljabri^g, Misbah Ashravi^a, Roaa A. Tayeb^h,
Mohammed M. Rahman^{i,*}

^a Department of Chemistry, University of Azad Jammu and Kashmir, Muzaffarabad 13100, Pakistan

^b Department of Biomedical and Environmental Engineering (BEE), California Innovations Corporation, 92037 San Diego, CA, USA

^c US-Pakistan Centre for Advanced Studies in Energy, National University of Science and Technology (NUST), 44000 Islamabad, Pakistan

^d Nanosciences and Technology Department (NS & TD), National Center for Physics (NCP), 44000 Islamabad, Pakistan

^e Department of Chemistry, King Abdulaziz University, P.O. Box 80203, Jeddah 21589, Saudi Arabia

^f Department of Physics, College of Science, Jazan University, P.O. Box 114, Jazan 45142, Saudi Arabia

^g Department of Chemistry, University College in Al-Jamoum, Umm Al-Qura University, Makkah 21955, Saudi Arabia

^h Department of Chemistry, College of Science, University of Jeddah, Alfaisaliah, Main girl campus, Jeddah, Saudi Arabia

ⁱ Center of Excellence for Advanced Materials Research (CEAMR) & Department of Chemistry, Faculty of Science, King Abdulaziz University, Jeddah 21589, Saudi Arabia

Received 21 December 2022; accepted 11 April 2023

Available online 18 April 2023

KEYWORDS

Graphene oxide;
Ternary metal oxides;
SnO₂-NiO-CuO nanocomposite;

Abstract Generally, Graphene oxide (GO) was fabricated by modified Hummer's method and was thermally reduced whereas the tri-metallic nanocomposite was prepared by ex-situ hybridization. Both the synthesized SnO₂-NiO-CuO (SNC) and rGO-SnO₂-NiO-CuO (GO-SNC) were calcined at 450 °C for 2 h. The degree of crystallinity and the crystallite size were examined through X-ray Diffraction (XRD) analysis and were found to increase with calcination temperature. The mor-

* Corresponding authors.

E-mail addresses: cii_raj@yahoo.com (S. Haq), mariaarashed555@outlook.com (M. Rashid), menaateam@gmail.com (F. Mena), nadia-shahzad@live.com (N. Shahzad), imran-shahzad@live.com (M. Imran Shahzad), salfaiifi@kau.edu.sa (S.Y.M. Alfaifi), osamam@jazanu.edu.sa (O. Madkhali), mdjabri@uqu.edu.sa (M.D. Aljabri), misbahchaudary999@gmail.com (M. Ashravi), ramtayeb@uj.edu.sa (R.A. Tayeb), mmrahman@kau.edu.sa (M.M. Rahman).

Peer review under responsibility of King Saud University.



Production and hosting by Elsevier

Antibacterial activity;
Antioxidant activity

phological changes were examined through scanning electron microscopy (SEM). The surface functional moieties were identified through Fourier transform infrared (FTIR) spectroscopy. Agar well diffusion method was used to evaluate samples against Gram-negative bacteria (*E. coli*) and Gram-positive bacteria (*S. aureus*). The antioxidant potential was analyzed against 2,2'-azino-bis(3-ethyl benzothiazoline-6-sulfonic acid (ABTS) and 2,2-diphenyl-1-picryl-hydrazyl-hydrate (DPPH) free radicals and the highest activity was found for the as-synthesized NC whereas a clear decrease was seen in both activities with after calcination at 450 °C. It was also observed that the antibacterial and antioxidant activities increased with increasing sample dose in the reaction.

© 2023 The Author(s). Published by Elsevier B.V. on behalf of King Saud University. This is an open access article under the CC BY license (<http://creativecommons.org/licenses/by/4.0/>).

1. Introduction

Huge number of bacteria resides as microflora on the surface and within the follicles of healthy human skin. The skin microbiome is made up of indigenous bacteria as well as fungal flora. Some of these indigenous organisms can overgrow and produce mild skin or appendage illness (Hay and Morris-jones 2017). Bacterial infection has become one of the world's major public health issues, recorded in millions of individuals every year. Antibacterial medications are now commonly utilized to combat this problem. However, the overuse of standard medicines has resulted in antibiotic resistant microbes, making treatment of the condition exceedingly challenging (Hamid et al. 2021). Antibiotic resistance is widespread among bacteria such as *Salmonella*, *E. coli*, *Staphylococcus aureus*, *Enterococcus*, and *Pseudomonas* species (Haq et al. 2020). Because these microbes can withstand traditional scientific therapy, antimicrobial drugs that are both safe and effective are required to defeat such resistant germs (Hamid et al. 2021) (Subhan et al. 2018) (Hossain et al. 2018). The advancement of nanotechnology has triggered the development of many nanoparticles for medicinal purposes (Haq et al. 2018a) (Uddin et al. 2015) (Subhan et al. 2019) (Asad et al. 2023). Researchers have looked into non-traditional antibacterial agents such as carbon nanotubes, metal nanoparticles, and metal oxide nanoparticles. Graphene has recently been presented as a new effective antibacterial material that has a significant cytotoxic impact on bacteria (Ji et al. 2016) (Subhan et al. 2020) (Hussain et al. 2022) (Khan et al. 2018).

Oxygen is the most essential element for the survival of biological system due to its oxidative properties. Besides being so helpful for the living system, it also intensifies the impairments within the cells in the form of free radicals. A molecule or segments of molecule that own non-bonding electrons in its valence orbital and exist independently are called free radicals. They are generated at the hand of a redox reaction and homolytic cleavage of a chemical bond which bring about chain reaction. Reactive nitrogen species (RNS) and reactive oxygen species (ROS) and other non-radical reactive derivatives falls in this category. Free radicals are very unstable and reactive species. They show multiple toxic effects in living system like destruction of tissues, ribonucleotide, DNA, cell membrane and biomolecules (Sen 2010). Free-radical oxygen species attack unsaturated acids in the cell membrane, causing harm to all living creatures. Superoxide dismutase, a protective enzyme, totally transforms these free-radical oxygen species into two water molecules and oxygen. However, activity of the enzyme declines with age. By scavenging radicals before they target the substrates, antioxidants serve a critical role in preventing oxidative damage. Therefore, developing novel catalysts for the removal of active radical species is in demand (Rehana et al. 2017) (Nanoparticles and Bedloví 2020). Some nanoparticles, transition metal oxide NCs, graphene and its derivatives and GO based metallic NCs play crucial part in free radical scavenging (Shadmehri et al. 2019) (Rajeswari and Prabu 2018) (Rakkappan and Halliah 2020) (Parsa and Salout 2016) (Menaar et al. 2021).

Graphene being a 'miracle material' is one of the most sensational materials that have been discovered till now. This smallest and strongest known material constitutes six membered rings of sp² hybridized carbon atoms. The atoms are extended in the two-dimensional layers which may be in the range 1–10 nm (Taghioskoui 2009) and C–C bond length is 0.142 nm (Singh et al. 2011). Graphene shows many extraordinary properties such as ballistic conduction of mobile electrons and ions that carries charge ($\sim 10000 \text{ cm}^2 \text{ V}^{-1} \text{ S}^{-1}$) at room temperature, Fractional Quantum Hall effect (QHE), extensive surface area ($2630 \text{ m}^2 \text{ g}^{-1}$), excellent optical transparency ($\sim 97.7 \%$), higher thermal conductivity ($3000\text{--}5000 \text{ W m}^{-1} \text{ K}^{-1}$), and high Young's modulus ($\sim 1 \text{ TPa}$). The graphene produces extended and definite derivatives such as rGO and GO which lead to the manufacturing of other effective materials (Huang et al. 2012). The honey comb lattice structure of graphene oxide constitutes epoxy and hydroxyl group on the two sides and carboxylic group on the edges (Jac 2017). As GO and rGO own some reactive oxygen containing groups which causes its further functionalization such as formulation of graphene-based composites (Huang et al. 2012). Graphene has been decorated with different metal and metal oxide NPs in attempt to improve its characteristics and widen its uses (Khan et al. 2015). Transition metal NPs have been fascinating in the present technological world because of their stability, crystallinity, and resistibility regulated shape with various morphologies. They are also used as antibacterial and antioxidant agents (Rakkappan and Halliah 2020) (Menaar et al. 2015). Metal nanoparticles (MNPs) and nanocomposites (MNCs) have been shown to have extraordinary antibacterial properties and can thus be employed in alternative medicines (Alavi and Rai 2019). Apart from improving graphene's characteristics, the NPs also function as a stabilizer, preventing individual graphene sheets from aggregating due to strong van der Waals interactions between the graphene layers (Khan et al. 2015).

Graphite is oxidized and exfoliated for the scalable synthesis of graphene oxide. Because the mechanical exfoliation procedures used to create graphene nanosheets are ineffective for large-scale production. The use of strong oxidizing agents to make GO is one of the most common techniques for graphite exfoliation. For the bulk scale production of graphene, chemical methods are a viable option (Alam et al. 2017). For this purpose, Brodie's method, Staudenmaier method, Hofmann method, and Hummer's method, as well as their modified and refined variants, are well-known approaches (Singh et al. 2016). Hummer's method is preferable because of its great efficiency and reaction safety. This approach has gotten a lot of attention because the process can be finished in a few of hours. Second, to avoid the formation of explosive ClO₂, KClO₃ was substituted with KMnO₄ (Alam et al. 2017). The GO based metallic NCs can be prepared by either ex-situ hybridization or in-situ crystallization. In ex situ hybridization, graphene-based nanosheets are mixed with pre-synthesized or commercially available nanocrystals in a solution. While in-situ crystallization can lead to homogeneous surface coverage of nanocrystals by regulating the nucleation sites on GO/rGO by surface functionalization (Huang et al. 2012).

Metal oxides attract the attention of the researcher due to their unique properties, such as high stability, high temperature resistance, and excellent electrical and optical properties. They have a wide range of applications in various fields, including electronics, catalysis, energy storage, and environmental remediation. Among the metal oxides, CuO is used as a catalyst in the production of methanol and as a semi-conducting material in electronics and optoelectronics applications, such as in the fabrication of solar cells, sensors, and transistors. It also has potential applications in the field of energy storage, such as in lithium-ion batteries (Derbalah et al. 2022). NiO is commonly used as a catalyst in various chemical reactions, such as in the production of hydrogen and the synthesis of organic compounds. It is also used in gas sensors and as a protective coating in electronic devices (Anand et al. 2020). SnO₂, as mentioned earlier, is widely used as a transparent conducting oxide (TCO) in electronics and optoelectronics applications due to its high conductivity and transparency. It is also used as gas sensors, photovoltaic devices, an electrode material in lithium-ion batteries, catalysts and also exhibits wide range biological applications (Bibi et al. 2020). The ternary systems of have metal oxides have gained increasing attention in material science due to their improved properties compared to unary and binary systems. The combination of three metal oxides in a ternary system can result in new and enhanced properties, such as increased catalytic activity, improved electrical conductivity, and higher thermal stability. This makes ternary systems an attractive area of research for developing new materials with tailored properties for specific applications (Ur Rehman et al. 2018).

The aim of this research is the synthesis of GO-SNC and SNC which proved as effective agents to knock down bacterial species and free radicals. Because of quick electron exchange and the existence of crystal defects, tri-metallic NPs interfaces have been more active so far, ensuring considerable implementation (Basavegowda et al. 2020). The lack of these composites in the literature was the driving force for the selection and coupling of these metals. The synthesized NCs were calcined at 450 °C and were fully characterized by FTIR, SEM, XRD, and DRS. The antibacterial efficacy was scrutinized against GNB (*E. coli*) and GPB (*S. aureus*). Moreover, free radical scavenging assay was performed against ABTS^{•+} and DPPH free radicals.

2. Materials and methods

2.1. Materials

Graphite, Phosphoric acid (H₃PO₄), 95–97 % conc. Sulfuric acid (H₂SO₄), potassium permanganate (KMnO₄), Hydrogen peroxide (H₂O₂), Hydrochloric acid (HCl), Nickel (II) sulfate hexahydrate (NiSO₄·6H₂O), Copper (II) sulfate pentahydrate (CuSO₄·5H₂O), tin (II) chloride 2-hydrate (SnCl₂·2H₂O), methanol (CH₃OH) and sodium hydroxide (NaOH) were obtained from sigma Aldrich. All the chemicals were of analytical grade and used without further purification. Deionized water (DIW) was utilized throughout the laboratory work. All the glassware was washed with DIW and then rinsed with acetone.

2.2. Preparation of GO

Modified Hummer's method was used to prepare GO from the graphite flakes. In this method 99 mL of H₂SO₄ was mixed with 11.0 mL of H₃PO₄ with volume ratio 9:1 and placed in an ice bath. The reaction mixture was stirred for 10 min at 10 °C. Then 2 g of graphite was added to the previous mixture under constant stirring followed by the slowly addition of 8 g

of KMnO₄. The obtained reaction mixture was stirred for 6 h until its color changed to dark green. Afterward, reaction mixture was stirred for 10 min after the addition of 6.0 mL of H₂O₂ to remove excess KMnO₄. An extensive care was required for this step because it was an exothermic reaction and released high amount of energy. So, this reaction took place in an ice-cold bath to maintain the temperature. The reaction was cooled down at room temperature. Then slowly added 13.0 mL of HCl in 39.0 mL of deionized with the volume ratio 1:3. Then this mixture was centrifuged for 10 min at 4000 rpm. The supernatant was decanted, and the residue was washed with HCl and then with DIW thrice to have its pH around 6 or 7. Finally, the obtained suspension was filtered and then dried in an oven for 24 h at 100 °C. The dried GO powder was black in color.

2.3. Preparation of SNC

For the preparation of nanocomposite of SNC, 3.78 g of SnCl₂·2H₂O, 4.48 g of NiSO₄·6H₂O and 3.93 g of CuSO₄·5H₂O were weighed separately. Then these metallic salts were added in the beakers contain 50.0 mL of DIW and 10 mL of methanol separately. Then these mixtures were stirred for 30 min at 50.0 °C. The pH of the solutions was maintained up to 10 by adding 2 M NaOH solution. All the three mixtures were combined together in a separate beaker and then kept on stirring for 3 h at 50 °C. The mixture was filtered with Whatman No. 1 filter paper. It was dried in an oven at 100 °C and then half of the sample was calcined at 450 °C for 2 h in muffle furnace.

2.4. Preparation of GO-SNC

For the synthesis of GO-SNC, GO was thermally reduced by sonicating 1.0 g of GO into 100 mL of DIW at 100 °C for 2 h. The rGO solution was poured slowly into the solution of previously prepared metallic nanocomposites and was kept on stirring for 4 h. The mixture was washed with DIW and filtered. The residue was dried in an oven at 100 °C. The resulting product in powdered form was GO-SNC. Half of the quantity of sample was calcined at 450 °C for 2 h.

2.5. Characterization

The properties of the synthesized SNC and GO-SNC were studied with the help of XRD, FTIR, and SEM. The FTIR (4000–400 cm⁻¹) was used to check chemical composition of whole sample using Nicolet 6700 (USA) (Dutta 2017). The XRD was performed by Panalytical X-pert Pro operated at 2-theta (20°–80°) to analyze crystalline structure and crystal phases of the sample (Epp 2016). SEM model 5910 made in Japan was used for the determination of surface topography and sample composition (Akhtar et al. 2018).

2.6. Antibacterial activity

The antibacterial activity of the samples was observed against a GPB (*S. aureus*) and a gram GNB (*E. coli*) via agar well diffusion method. These bacterial strains were collected from the department of Biotechnology, University of AJ&K, Muzaf-

farabad. The apparatus used was sterilized in autoclave. For comparative study, suspensions of various concentrations i.e., 10, 20, 30, 40, 50, 60 mg/3mL were prepared in DIW. The laminar flow was used to perform the activity which was sanitized with the 70 % ethanol solution. Nutrient agar fluid was spread into the petri dishes and allowed to solidify. Afterwards, 50.0 μ L of prepared bacterial media was spread on it with micropipette and evenly distributed by swabbing. Sterile microtips were used to bore wells of 5 mm in it and sterile needles were used to eliminate agar plugs. Then, 30.0 μ L of each prepared suspension, positive and negative controls, were filled in the separate wells. The petri dishes were placed into an incubator at 37 °C for 16 h. Thus, the zones of inhibitions of calcined and uncalcined samples of SNC and GO-SNC, rGO, graphite and DIW were measured. Finally, in a separate petri dish, same procedure was followed for the calcined samples of SNC and GO-SNC, graphite and water along with an antibiotic. As, they showed highest antibacterial activity at highest concentration, that is why 30.0 μ L of each 60 mg/3mL of suspensions were used and then zones of inhibition were measured. Similar procedure was followed for uncalcined samples of SNC and GO-SNC. Likewise, the zones of inhibitions of calcined and uncalcined samples of SNC and GO-SNC were measured against selected bacteria. The solvent (water) as used as negative control whereas the ciprofloxacin was used as positive control.

2.7. Antioxidant activity

Antioxidant activity was performed to examine the potential of calcined and uncalcined samples of SNC and GO-SNC to stabilize ABTS and DPPH free radicals. Various concentrations (5, 10, 15 and 20 μ g) of calcined and uncalcined samples were dissolved in 5 mL of DIW and sonicate for 30 min to form suspension. Aqueous solutions of 5.0 mM of potassium persulphate and 14 mM ABTS were prepared individually. Afterwards, these freshly prepared suspensions were mixed in 1:1 V/V and kept in dark for 16 h at room temperature to get blue green solution of ABTS free radical ($\text{ABTS}^{\bullet+}$). While DPPH \bullet stock solution was made by dissolving 4.0 mg of DPPH in 50 mL methanol. The resultant deep purple solution was kept for half an hour in dark to get DPPH free radical (DPPH \bullet).

2.7.1. ABTS free radical scavenging

50 μ L of each test solutions of nanocomposites were added into the separate test tubes through micropipette. 1.0 mL of $\text{ABTS}^{\bullet+}$ solution was added in each test tube and kept in dark for half an hour. Firstly, the absorbance of $\text{ABTS}^{\bullet+}$ solution was measured at 734 nm through UV-visible spectrophotometer while keeping distilled water in the reference cell. Later on, the absorbance of samples was measured at the same wavelength.

2.7.2. DPPH free radical scavenging

The procedure revealed in section 2.7.1 was followed to examine the DPPH \bullet scavenging of the nanocomposites. But the wavelength was set to be 517 nm and methanol was taken in the reference.

2.7.3. Ascorbic acid as standard antioxidant

Ascorbic acid was used as a standard for the comparative analysis of the samples with previously known potent antioxidant. The antioxidant activity of ascorbic acid was done against both ABTS and DPPH free radical and absorbance was measured at 734 nm and 517 nm respectively.

2.7.4. Percent radical scavenging activity

The percentage scavenging activity of the calcined and uncalcined samples of SNC and GO-SNC against DPPH and ABTS free radical was measured by followed equation (1): where A_i is the absorbance of sample and A_o is the absorbance of control (Rehman et al. 2021).

$$\% \text{radical scavenging potential} = \frac{A_o - A_i}{A_o} \times 100 \quad (1)$$

3. Results and discussion

3.1. XRD analysis

The XRD technique was used to examine the crystalline structure and the chemical composition of the synthesized GO, SNC and GO-SNC. The XRD spectrum given in Fig. 1, exhibits a diffraction peak at 10.78°, which corresponds to the interlayer d-spacing of 8.17 Å, which is almost similar to those reported earlier and this diffraction x-ray correspond to (111) plane as given in reference card number 01-082-2261. The determined density was found to be 2.12 g/cm³ where the volume of cell was found to be 2834.35 $\times 10^6$ pm³. It has been evident from the literature, that the peaks for graphite flakes are not appeared in the XRD pattern of GO which suggest that all the graphite was successfully converted into GO.

The XRD pattern of the un-calcined and calcined SNC and GO-SNC are given in the Fig. 2. The pattern for un-calcined nanocomposite beside a sharp signal at 36.55° ascribed to (551) plane is much noisy suggesting that most the sample is amorphous. However, upon heating, several reflections have been appeared in the diffractogram at 2 θ angle of 23.26, 33.06, 36.55, 42.46, 47.41 and 61.76 due to the miller planes

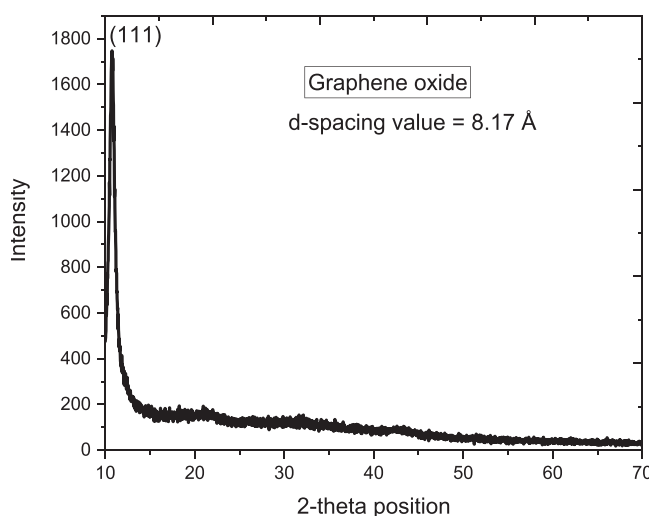


Fig. 1 XRD pattern of synthesized GO.

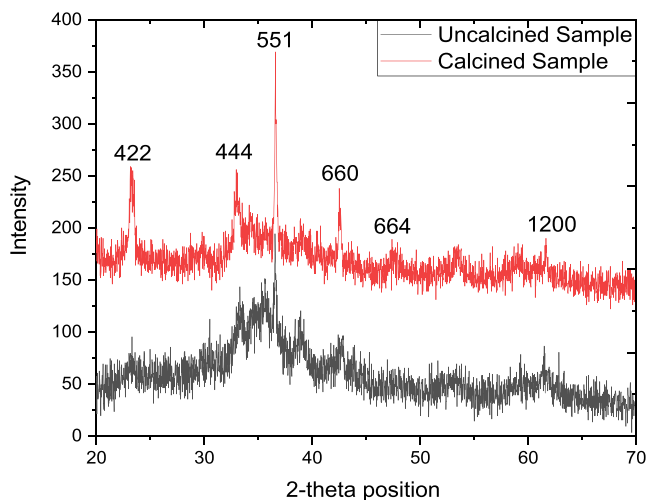


Fig. 2 XRD pattern of both uncalcined and calcined SNC.

(422), (444), (551), (660), (664) and (1200) respectively. All these diffraction bands are matched with reference card no 00-030-0496, confirm the synthesis of Cu, Ni and Sn nanocomposite with chemical formula of Cu_9NiSn_3 with cubic geometrical shape with space group of F-43 m. The length of all three coordinates of the cubic are of 1.801 nm with 90° of alpha, beta and gamma. The average crystallite size calculated by Debye-Scherrer equation is 14 nm, where 0.75 % imperfection was found in the crystal.

The XRD pattern of the GO/ Cu_9NiSn_3 nanocomposite (both un-calcined and calcined) are shown in the Fig. 3, which displays the diffraction peak at 2 θ position as that were observed in the XRD spectrum of Cu_9NiSn_3 nanocomposite as shown in Fig. 3. No shift was seen in the position of diffraction bands is the evidence that the Cu_9NiSn_3 was only incorporated on graphene oxide sheet and chemical linkage was formed. However, the d-spacing value for the plane (551) is 2.523 Å in case of pure Cu_9NiSn_3 nanocomposite whereas this value decreases to 2.458 Å which confirm the incorporation of graphene oxide on the Cu_9NiSn_3 nanocomposite. This shifting

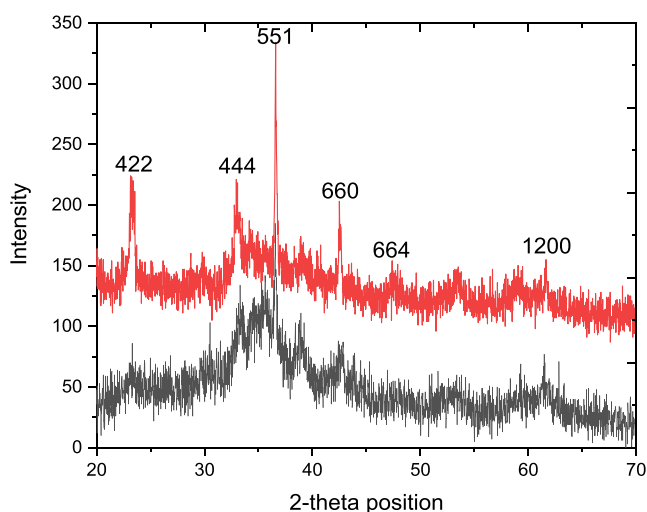


Fig. 3 XRD pattern of both uncalcined and calcined GO-SNC.

of d-spacing to lower value is because of the reorganization of the lattice position after the mixing of GO and Cu_9NiSn_3 nanocomposite. As the ionic radii of the Cu^{2+} , Ni^{2+} and Sn^{4+} is larger and the space between is larger and after the incorporation of GO, the carbon with small ionic radius adjusted between the metal atoms led the reduction of d-spacing. The average crystallite size increase from 14 nm to 57.45 nm and the lattice strain reduced to 0.59 %, proposed that after the incorporation of GO, the nanocomposite become more stable.

3.2. SEM analysis

The SEM image shown in Fig. 4(a) described the morphological features of the synthesized GO, where a layer type structure were detected. The multilayers structure of the GO is observed that has high surface roughness. The cavities/cracks are seen in the GO sheets which might be due to the grinding of the sample after dehydration. The morphological study of the as-synthesized and calcined Cu_9NiSn_3 nanocomposite was conducted through SEM analysis and the micrographs are shown in Fig. 4(b and c). The snowball-like structures (grains) that are observed in the micrograph (4b) can result from the aggregation of smaller particles, which are formed during the synthesis process. These snowball-like structures are irregular dispersion are clump together, forming larger structures led to the size vibration of the particles. The background of the sample shows high degree of agglomeration, which may be due to high surface energy of the particles which held the particles together. The calcination of sample at high temperature can cause the individual snowball-like structures (grain) in the sample to grow by diffusion-driven processes, such as grain boundary migration and recrystallization. The growth of the individual grains can result in an increase in the average grain size of the sample. The cavities of distinct size are formed due to the irregular arrangement of these grains. The grain size for as-synthesized estimated from the SEM images is ranging from 40.75 to 98.93 nm with average size of 84.55 nm, whereas those for calcined sample ranging from 68 to 123 nm with average size of 101 nm. The SEM analysis was also carried out after the incorporation of metals (Cu, Ni and Sn) in the GO matrix to examine the effect on the morphology of the resultant composite. The obtained SEM images are shown in Fig. 4(d and e), reveals that the morphology of the sample is completely changed after mixing of metals and GO. The metal nanocomposite deeply incorporated in GO layer, which have changed the morphology of the sample. The as-synthesized sample shows that the grains are embedded in the GO layer, where majority of the cavities that seen in the Cu_9NiSn_3 NC (Fig. 4(b)) have been filled due to the deposition of GO. Upon calcination, the GO layer became more prominent and converted to a semi porous sheet and boundaries between copper nickel tin nanocomposite grains are almost disappeared.

3.3. FTIR analysis

In order to describe the bond structure of rGO, calcined and uncalcined SNC and GO-SNC transmission spectra of KBr sample pellets were acquired using Fourier transforms infrared spectroscopy (FTIR). The Figs. 5, 6 and 7 shows the FTIR

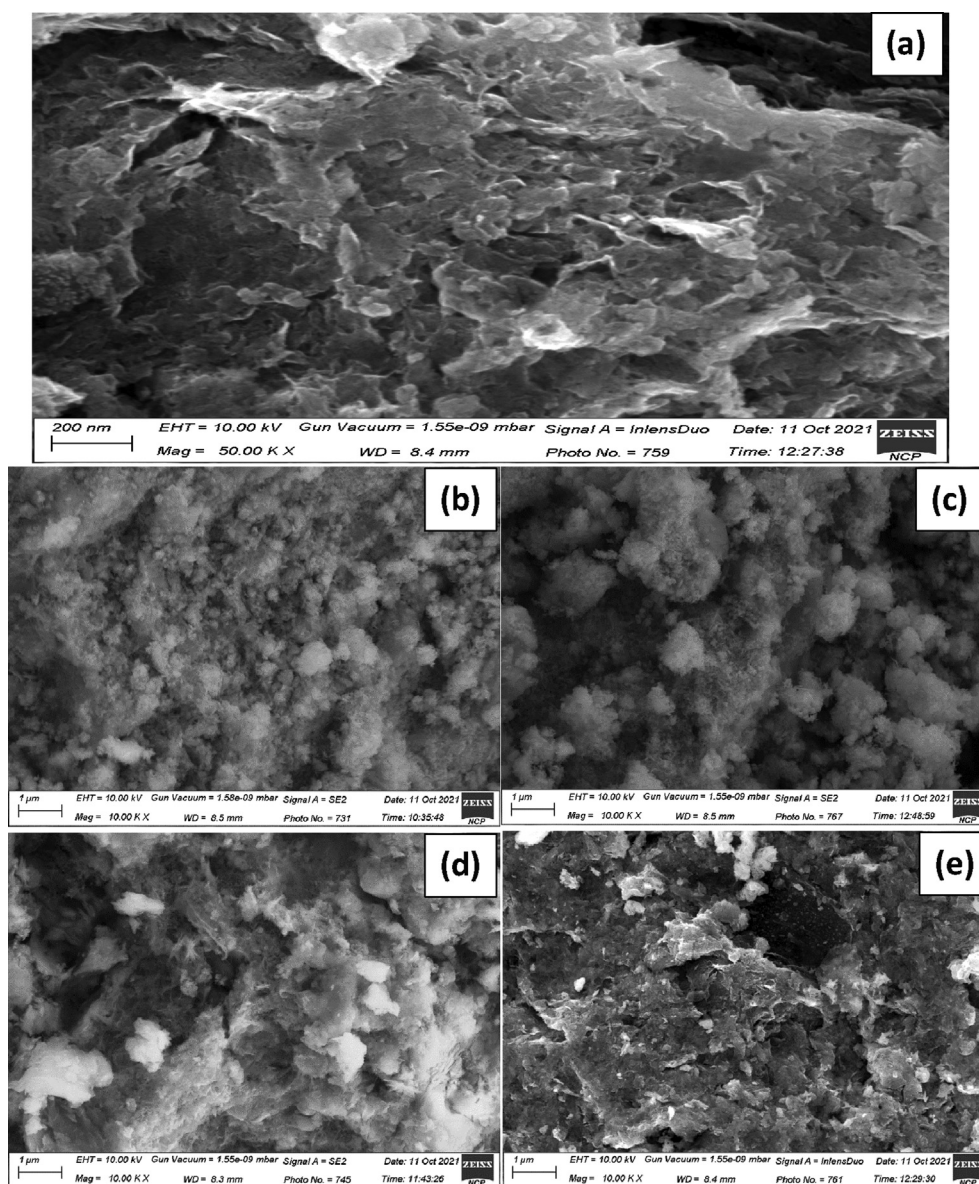


Fig. 4 SEM images of GO (a), as-synthesized (b) and calcined (c) of SNC; as-synthesized (d) and calcined (e) of GO-SNC.

spectrum of the GO, SNC (both uncalcined and calcined) and GO-SNC (both uncalcined and calcined) in the range of 3800 to 550 cm^{-1} . In FTIR plot of GO (Fig. 5), two peaks were observed at 3404.10 cm^{-1} correspond to the stretching vibration of O–H (N. Baali, A. Khecha 2019). The peaks at 2929.68 cm^{-1} and 2834.47 cm^{-1} indicated the symmetric and asymmetric stretching of the C–H group respectively (Parthipan et al. 2021). The peak at 2308.34 cm^{-1} referred to the C = O group (O = C = O) the node at 1717.37 cm^{-1} attributed to C = C vibrations (Ebnalwaled et al. 2019). The peaks located at 1607.38 cm^{-1} is related to the C = C of aromatic ring whereas the peaks at 1381.66 cm^{-1} and 1118.19 cm^{-1} are assigned to C = C and C–O moieties, respectively (Alam et al. 2017). The peak at 600.27 cm^{-1} is might be due to the out plane bending vibration of C–H moiety (Shahriary Leila and Athawale Anjali A. 2014; Yoo and Park 2019).

FTIR spectroscopic analysis of SNC (uncalcined and calcined) shows (Fig. 6) the peak in the range of 3524.18 cm^{-1} shows the vibration of non-bonding water molecules adsorbed on the surface of sample (Shah et al. 2023). The band at 3473 cm^{-1} corresponds to the stretching vibration of OH group due to the fact that calcined powder tends to physically absorb water. The intensity of these peak decrease after the calcination, suggest the evaporation of water molecules from the same. The peak at 1385.83 cm^{-1} correspond to the C = O stretching vibration (El-Kemary et al. 2013). The peak attributed at 1044.60 cm^{-1} correspond the Cu–O–Cu vibration (Sorbiun et al. 2018). The peak at 571.72 cm^{-1} correspond to Ni–O stretching vibration (Haq et al. 2021c). The peak at 887.58 cm^{-1} ascribed C–C vibration (Al-Hada et al. 2018).

The FTIR analysis of GO-SNC (uncalcined and calcined) shows a wide wave band centered at 3398.46 cm^{-1} shows that O–H stretching vibration (Fig. 7) and the decrease intensity of

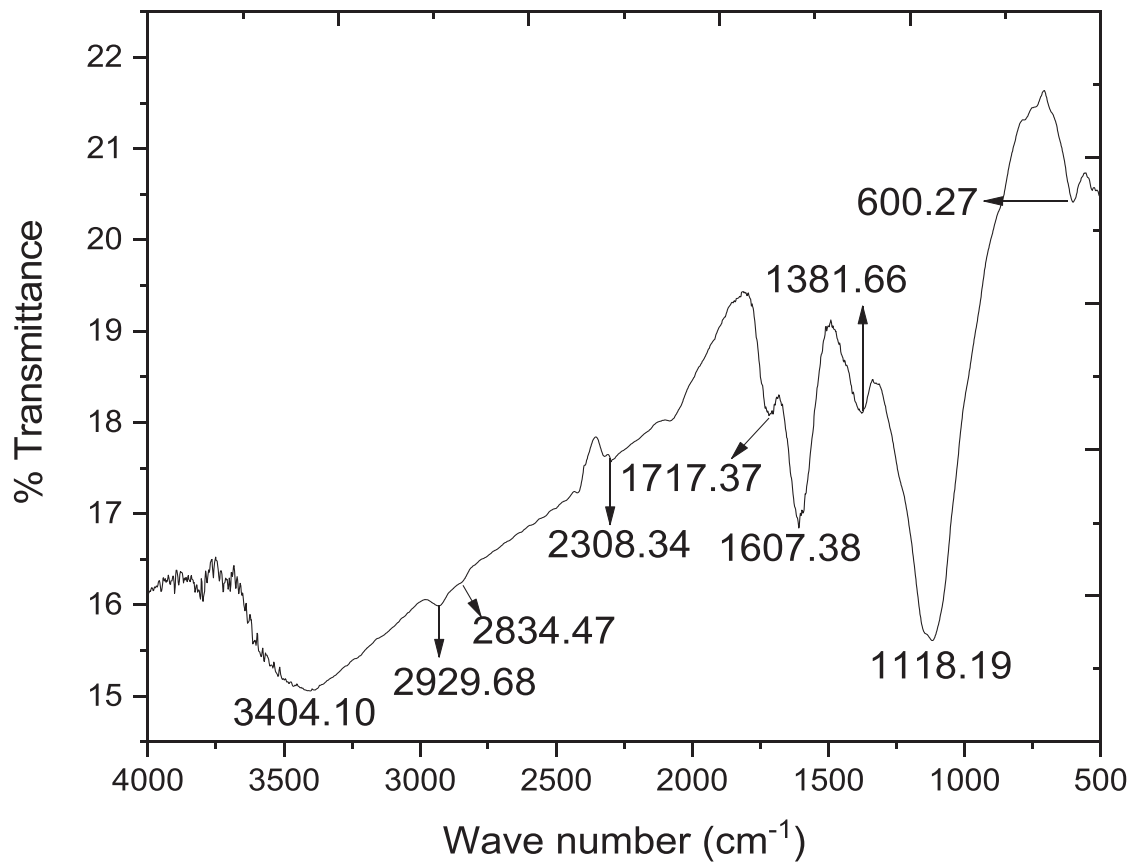


Fig. 5 FTIR spectrum of the synthesized GO.

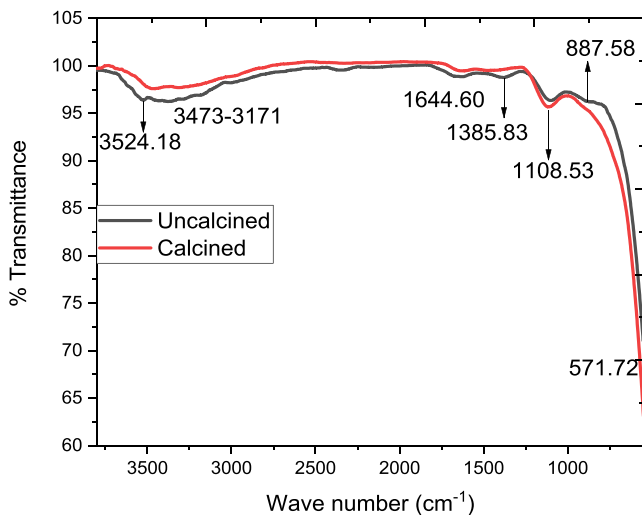


Fig. 6 FTIR spectrum of the uncalcined and calcined SNC.

this peak decrease after the calcination, suggest the evaporation of water molecules from the same. The peak at 1624.89 cm^{-1} correspond to the $\text{C}=\text{O}$ vibration (Haghshenas et al. 2019). The peak at 1490.30 cm^{-1} ascribed C-O-C vibration (Haq et al. 2018b). The peak at 1362.47 cm^{-1} due to the vibration of $\text{O}-\text{C}=\text{O}$ group (Paquin et al. 2015). The peak at 1028.36 cm^{-1} show the Cu-O-Cu vibration (Hamid et al. 2021). The peak at

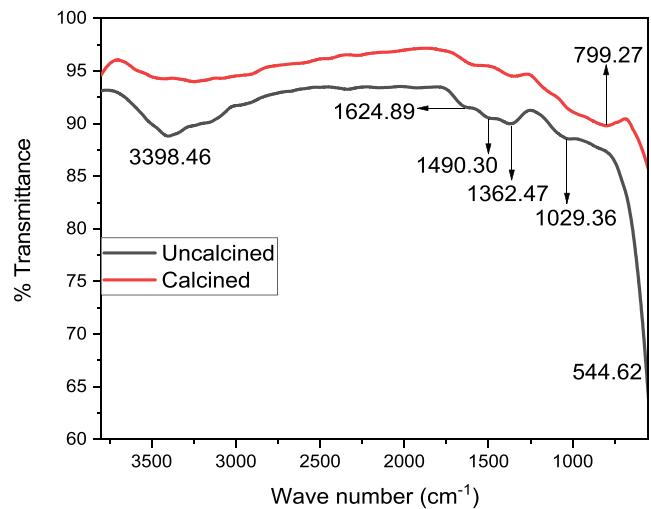


Fig. 7 FTIR spectrum of the uncalcined and calcined GO-SNC.

544.63 cm^{-1} attributed to the Ni-O vibration (Haq et al. 2021c). The peak at 799.27 cm^{-1} show the Sn-O stretching vibration (Shoukat et al. 2019).

3.4. Antibacterial activity

The uncalcined and calcined of SNC and GO-SNC were tested against Gram-positive and Gram-negative bacteria. Agar well

diffusion method was used to evaluate the antibacterial activity of samples under study. *E. coli* and *S. aureus* were selected as GNB and GPB respectively. The inhibition zones showing (Fig. 8) bactericidal activity were measured in millimeter (mm) show in Table 1. The microbial activity of samples was analyzed at different concentrations of 10, 20, 30, 40, 50, and 60 $\mu\text{g/mL}$. It was examined that bacterial activity was directly related to the concentration of samples. As in aqueous solution, metallic nanocomposites form metal cations, hydroxyl radical, superoxide radical anions. The cations are reactive towards the thiol group of fundamental bacterial enzyme. This interaction caused the inactivation of cell activities which lead to the cell death. However, radicals thus formed interact with

the cell surface which is negatively charged. Therefore, cell wall ruptured and caused loss of cell content which inhibited cell growth (Haq et al. 2021a). Likewise, aqueous suspensions of tested samples generated reactive species to more extent by increasing concentration per mL. This resulted in increase in the inhibition capacity of the sample against bacteria.

It was observed that GO-SNC showed higher antibacterial activity than SNC against GNB and GPB. GO supported metallic nanocomposites show higher antibacterial activity as compared to bare metallic nanocomposites (Ahmad et al. 2016). The oxygen vacancy present at the GO surface which can act as sorption center of water molecules will react with water molecules thus resulting in the formation of the hydroxyl

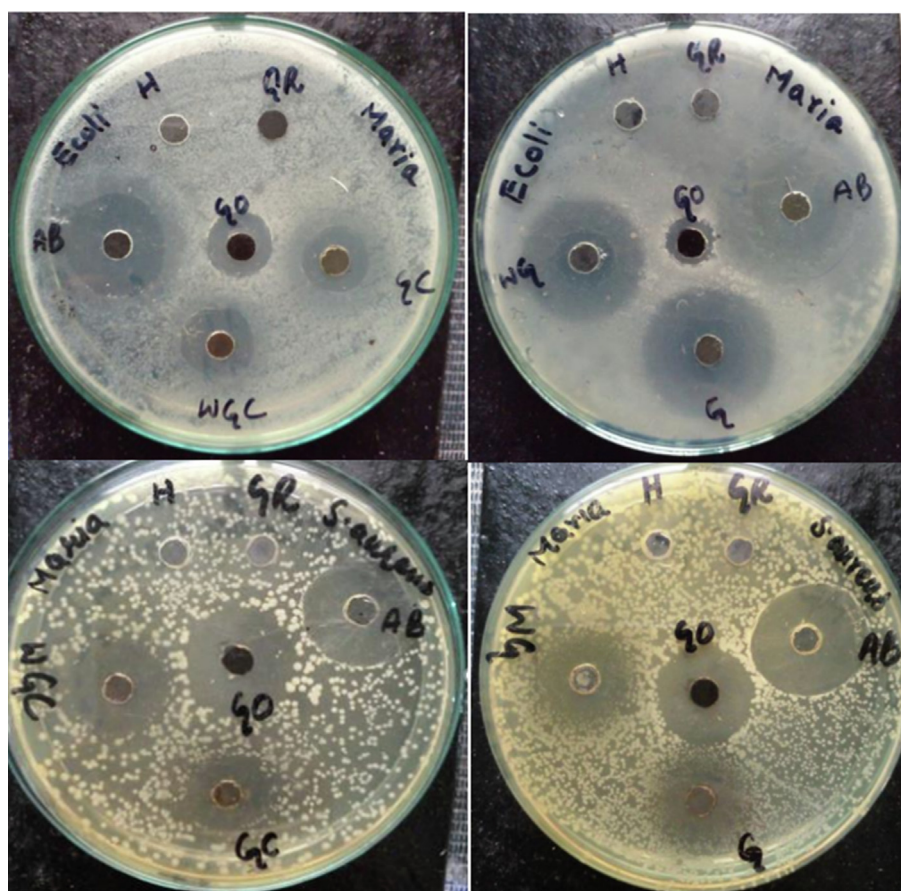


Fig. 8 Antibacterial activity of uncalcined and calcined SNC and GO-SNC; H = -ve control (solvent), AB = +ve control (Antibiotic), GO = graphene oxide, G = GO-SNC, WG = SNC, GC = calcined GO-SNC, and WGC = calcined SNC.

Table 1 Antibacterial activity of uncalcined and calcined sample of SNC and GO-SNC.

Samples	Zones of inhibition in millimeters (mm)			
	<i>E. coli</i>	Standard deviation	<i>S. aureus</i>	Standard deviation
GO	6	1	15	1.58
Antibiotic	16	1.64	20	1.83
GO-SNC	24	2	16	1.64
GO-SNC calcined	9	1.23	12	1.42
SNC	21	1.88	7	1.09
SNC calcined	11	1.36	15	1.59

radicals. The direct contact of graphene sheets edges and metal ions ruptures the bacterial cell to form pores. In this way there occur losses of cytoplasmic material which inhibit the growth of bacteria. Furthermore, bacteria's can be entrapped into graphene sheets which causes inactivation of bacterial cells. Moreover, GO sheets trap the bacterial cell and isolate it from its environment. In this way, bacterial growth is retarded due to inactivation of cell system (Ji et al. 2016).

The zones of inhibition of calcined samples of SNC and GO-SNC were reduced as compared to uncalcined ones. The potential explanation of this behavior could be the particle size. Upon calcination, particle size increased and surface area to volume ratio decreased. As a result, reactive sites of the particles reduced which gave rise to the less interaction of NCs with the bacterial surfaces. While in uncalcined samples, surface area of the NCs was large because of the smaller size of nanoparticles. Consequently, NCs strongly interacted with the bacterial cell wall. In this way, bacterial cell death became easier and maximum zones of inhibition were observed (Hamid et al. 2021).

The prepared NCs showed greater zones of inhibition against GNB as compared to GPB. It is attributed to the variation in chemical composition of each bacterial cell wall. GPB have thick layer of peptidoglycan in cell wall which strongly resist the penetration of foreign particles into the cell. Whereas the outer layer of GNB contains thin layer of peptidoglycan and its extent of resistance is low which led to the penetration of particles through the cell wall. Another possible reason for enhanced activity of NCs against GNB was due to the strong interaction of metal cations with the highly negative surface of bacteria. The teichoic acid in the cell wall of GPB makes its surface to be partially negative, thus have weaken interaction between cations and bacteria. The less interaction is responsible for the increased resistance of GPB against the tested samples (Haq et al. 2021b).

The obtained antibacterial activity results against both bacteria were compared with available the literature. The GO based trimetallic oxide nanocomposites are not reported yet. However, antibacterial activity of GO based monometallic and bimetallic nanocomposites against both *E. coli* and *S. aureus* are reported and the zones of inhibition are listed in Table 2. The listed results shows that the GO based trimetallic nanocomposite reported in this study is more active than the composites reported in literature.

3.5. Antioxidant activity

The manifestation of free radical scavenging potential of molecules against sustained free radical reduction is the key princi-

ple of antioxidant action. The antioxidant potential of prepared NCs was analyzed against DPPH and ABTS free radicals at different concentrations as shown in Table 3 and Table 4. Both of these unstable free radicals were reduced by the target sample. Therefore, reduction leads to the stabilization of the unstable free radicals. With increasing the concentration of the sample, the absorbance was found to be decreasing. Decrease in absorbance revealed the free radical scavenging activity of the sample. Accordingly, percentage radical scavenging activity of the sample kept on increasing. It was observed that antioxidant activity of the sample increased with increasing the sample dose. This increased antioxidant activity is attributable to a greater concentration of sample that can oppose more reactive oxygen species (DPPH and ABTS) (Haq et al. 2020).

It was also observed that GO-SNC nanocomposite show more antiradical efficacy as compared to SNC. This might be explained by the production of a radical adduct at sp^2 car-

Table 3 Antioxidant activity of the GO, SNC and GO-SNC against ABTS free radical.

Samples	Concentration mg/mL	%RSA	IC ₅₀
GO	0.005	90.35	14.82
	0.010	92.39	
	0.015	93.57	
	0.020	98.25	
SNC	0.005	83.04	32.43
	0.010	89.18	
	0.015	93.86	
	0.020	96.78	
SNC calcined	0.005	41.52	42.33
	0.010	67.25	
	0.015	75.73	
	0.020	81.58	
GO-SNC	0.005	83.92	24.56
	0.010	86.84	
	0.015	88.59	
	0.020	93.86	
GO-SNC calcined	0.005	52.22	45.43
	0.010	59.35	
	0.015	62.86	
	0.020	82.46	
Ascorbic acid	0.005	33.04	41.81
	0.010	37.42	
	0.015	40.35	
	0.020	44.15	

Table 2 Comparison of antibacterial activity of the recently reported data with available literature.

Samples	Zones of inhibition in millimeter (mm)		References
	<i>E. coli</i>	<i>S. aureus</i>	
FRGO-Ag/AgO/Ag ₂ O	16	15	(Lekshmi et al. 2022)
cellulose/GO/CuO	12.7	16.3	(Xie et al. 2020)
GO@ZnO	0.05	0.025	(Ray Chowdhuri et al. 2015)
GO@CS/ZnO	0.0025	0.005	(Ray Chowdhuri et al. 2015)
ZnO:Cu:Graphene	16	16	(Ravichandran et al. 2016)
rGO-SnO ₂ -NiO-CuO	24	16	Present work

Table 4 Antioxidant activity of the GO, SNC, and GO-SNC against DPPH free radical.

Samples	Concentration mg/mL	%RSA	IC ₅₀
GO	0.005	89.68	15.98
	0.010	94.94	
	0.015	97.08	
	0.020	99.02	
SNC	0.005	73.93	36.55
	0.010	76.07	
	0.015	81.32	
	0.020	88.91	
SNC calcined	0.005	53.51	36.98
	0.010	57.97	
	0.015	61.28	
	0.020	65.17	
GO-SNC	0.005	76.85	33.68
	0.010	79.96	
	0.015	81.71	
	0.020	90.86	
GO-SNC calcined	0.005	42.02	46.18
	0.010	50.39	
	0.015	59.14	
	0.020	68.09	
Ascorbic acid	0.005	69.26	22.33
	0.010	71.40	
	0.015	73.92	
	0.020	76.45	

bon sites, which then results in radical annihilation. The production of a second adduct occurs as a result of spin delocalization across the conjugated backbone of graphene. Electron transport and hydrogen donation from hydroxyl functional groups connected to graphene are also significant. Despite the fact that the basal plane of graphene acts as the primary scavenging location, hydrogen donation from oxygen-containing functional groups is still a significant factor in radical scavenging instance (Hastak et al. 2018). GO-SNC had higher antioxidant activity than SNC, which might be attributed to synergetic effects between SNC and GO. Because of the characteristics of SNC and GO, GO-SNC might form reactive oxygen species. These species donate electrons to the free radicals thus making them stable (Shadmehri et al. 2019).

The antioxidant results were obtained against both DPPH and ABTS free radicals. In both cases, calcined and uncalcined samples of SNC and GO-SNC showed increased in percentage scavenging activity with increasing sample dose. In comparison to calcined sample, the percentage scavenging activity of uncalcined sample was greater. The IC₅₀ value of a sample refers to the concentration of that sample required to scavenge the 50% of free radical. The uncalcined samples have less IC₅₀ value as compared to calcined sample. Comparatively, samples having less IC₅₀ values reveal higher antioxidant potential. In case of both scavenging assays, the uncalcined sample showed higher antioxidant activity. This is because the particle size increases with the rise in temperature. Increase in the particle size leads to decrease in number of nanoparticles in solution. Due to the less number of particles, less active sites will be available to stabilize the free radicals (Haq et al. 2021c).

4. Conclusion

The goal of this research is to create biologically active novel compounds and test them for various biological applications. The method for producing reduced graphene oxide from graphite is straightforward, but it necessitates extreme caution due to its exothermic nature. Different techniques were used to synthesized SNC and GO-SNC. The NCs were synthesized (calcined at 450 °C), which was then characterized by different techniques. After an extensive review of literature, it is confirmed that these composites are not reported previously. The successful synthesis was confirmed using XRD and FTIR analysis, with the XRD results indicating that the physicochemical properties improved significantly after calcination. The surface morphology was also investigated, with the results revealing the formation of larger aggregates of various sizes and shapes. The metal oxide appears to be embedded in the graphene matrix, according to SEM analysis. The agglomeration seen in SEM of SNC was gone in GO-SNC because it was stirred for a long time, which helped to separate the larger aggregates into individual particles. Following standard protocols, the potency of the synthesized GO, SNC, GO-SNC and their calcined counterpart was tested against Gram-positive and Gram-negative bacteria, as well as free radicals of ABTS and DPPH. All of these activities were found to increase with increasing sample concentration in the experimental procedure, implying that higher sample concentrations result in more activity. The activity of GO-SNC and its calcined analogue was found to be higher than the activity of calcined and uncalcined SNC among the samples. Antibacterial and antioxidant activities were performed in comparison to standard antibiotic and antioxidant. Ascorbic acid as standard antioxidant against ABTS and DPPH free radicals was found to be less than GO but higher than SNC and GO-SNC, and their calcined counterparts. After the careful evaluation of the calcined and uncalcined SNC and GO-SNC, it is concluded that these compounds may also be used in the future for environmental pollution remediation and catalytic processes.

Acknowledgment

This research work was funded by Institutional Fund Projects under grant no (IFPIP-540-130-1443). The authors gratefully acknowledge technical and financial support provided by the ministry of Education and King Abdulaziz University, DSR, Jeddah, Saudi Arabia.

References

- Ahmad A, qureshi AS, Li L, et al (2016) Antibacterial activity of graphene supported FeAg bimetallic nanocomposites. *Colloids and Surfaces B: Biointerfaces* 143:490–498. doi: 10.1016/j.colsurfb.2016.03.065
- Akhtar K, Khan SA, Khan SB, Asiri AM (2018) Scanning electron microscopy: Principle and applications in nanomaterials characterization.
- Alam, S.N., Sharma, N., Kumar, L., 2017. Synthesis of Graphene Oxide (GO) by modified hummers method and its thermal reduction to obtain Reduced Graphene Oxide (rGO)*. *Graphene* 06, 1–18. <https://doi.org/10.4236/graphene.2017.61001>.
- Alavi, M., Rai, M., 2019. Recent advances in antibacterial applications of metal nanoparticles (MNPs) and metal nanocomposites (MNCs) against multidrug-resistant (MDR) bacteria. *Expert Rev. Anti Infect. Ther.* 17, 419–428. <https://doi.org/10.1080/14787210.2019.1614914>.
- Al-Hada, N.M., Kamari, H.M., Baqer, A.A., et al, 2018. Thermal calcination-based production of SnO₂ nanopowder: an analysis of SnO₂ nanoparticle characteristics and antibacterial activities. *Nanomaterials* 8, 1–18. <https://doi.org/10.3390/nano8040250>.

- Anand, G.T., Nithiyavathi, R., Ramesh, R., et al, 2020. Structural and optical properties of nickel oxide nanoparticles: Investigation of antimicrobial applications. *Surf. Interfaces* 18,. <https://doi.org/10.1016/j.surfin.2020.100460> 100460.
- Asad, M., Arshad, M.N., Asiri, A.M., Rahman, M.M., Snigdha, K., Musthafa, T.N.M., 2023. Chitosan-Cu catalyzed novel ferrocenated spiropyrrolidines: green synthesis, single crystal X-ray diffraction, Hirshfeld surface and antibacterial studies. *Polymers* 15, 429.
- N. Baali, A. Khecha AB et al. (2019) Assessment of Antioxidant Activity of Pure Graphene Oxide (GO) and ZnO-Decorated Reduced Graphene Oxide (rGO) Using DPPH Radical and H₂O₂ Scavenging Assays. *C-Journal of Carbon Research* 5:75
- Basavegowda, N., Patra, J.K., Baek, K.H., 2020. Essential oils and mono/Bi/tri-metallic nanocomposites as alternative sources of antimicrobial agents to combat multidrug-resistant pathogenic microorganisms: an overview. *Molecules*. <https://doi.org/10.3390/molecules25051058>.
- Bibi, N., Haq, S., Rehman, W., et al, 2020. Low temperature fabrication of SnO₂, ZnO and Zn₂SnO₄ nanostructures for the degradation of Rhodamine 6G: characterization. *Biointerface Res. Appl. Chem.* 10, 5895–5900.
- Derbalah, A., Abdelsalam, I., Behiry, S.I., et al, 2022. Copper oxide nanostructures as a potential method for control of zucchini yellow mosaic virus in squash. *Pest Manag. Sci.* 78, 3587–3595. <https://doi.org/10.1002/ps.7001>.
- Dutta, A., 2017. *Fourier Transform Infrared Spectroscopy*. Elsevier Inc..
- Ebnalwaled, A.A., El-Fadl, A.A., Tuhamy, M.A., 2019. Characterization studies of reduced graphene oxide/zinc oxide nanocomposites synthesized by hydrothermal method. *J. Mater. Appl.* 8, 80–90. <https://doi.org/10.32732/jma.2019.8.2.80>.
- El-Kemary, M., Nagy, N., El-Mehasseb, I., 2013. Nickel oxide nanoparticles: synthesis and spectral studies of interactions with glucose. *Mater. Sci. Semicond. Process.* 16, 1747–1752. <https://doi.org/10.1016/j.mssp.2013.05.018>.
- Epp, J., 2016. *X-Ray Diffraction (XRD). Techniques for Materials Characterization*. Elsevier Ltd..
- Haghshenas, S.S.P., Nemati, A., Simchi, R., Kim, C.U., 2019. Photocatalytic and photoluminescence properties of ZnO/graphene quasi core-shell nanoparticles. *Ceram. Int.* 45, 8945–8961. <https://doi.org/10.1016/j.ceramint.2019.01.226>.
- Hamid, A., Haq, S., Ur Rehman, S., et al, 2021. Calcination temperature-driven antibacterial and antioxidant activities of fumaria indica mediated copper oxide nanoparticles: characterization. *Chem. Pap.* 75, 4189–4198. <https://doi.org/10.1007/s11696-021-01650-7>.
- Haq, S., Rehman, W., Waseem, M., et al, 2018a. Effect of heating on the structural and optical properties of TiO₂ nanoparticles: antibacterial activity. *Appl. Nanosci.* <https://doi.org/10.1007/s13204-018-0647-6>.
- Haq, S., Rehman, W., Waseem, M., et al, 2018b. Fabrication of pure and moxifloxacin functionalized silver oxide nanoparticles for photocatalytic and antimicrobial activity. *J. Photochem. Photobiol. B Biol.* 186, 116–124. <https://doi.org/10.1016/j.jphotobiol.2018.07.011>.
- Haq, S., Rehman, W., Waseem, M., et al, 2020. Green synthesis and characterization of tin dioxide nanoparticles for photocatalytic and antimicrobial studies. *Mater. Res. Express* 7, 10. <https://doi.org/10.1088/2053-1591/ab6fa1>.
- Haq, S., Abbasi, F., Ben Ali, M., et al, 2021a. Green synthesis of cobalt oxide nanoparticles and the effect of annealing temperature on their physiochemical and biological properties. *Mater. Res. Express* 8,. <https://doi.org/10.1088/2053-1591/ac1187> 075009.
- Haq, S., Ahmad, P., Khandaker, M.U., et al, 2021b. Antibacterial, antioxidant and physicochemical investigations of tin dioxide nanoparticles synthesized via microemulsion method. *Mater. Res. Express*. <https://doi.org/10.1088/2053-1591/abed8a>.
- Haq S, Dildar S, Ali M Ben, et al (2021c) Antimicrobial and antioxidant properties of biosynthesized of NiO nanoparticles using Raphanus sativus (R. sativus) extract. *Materials Research Express*. doi: 10.1088/2053-1591/abfc7c.
- Hastak, V., Bandi, S., Kashyap, S., et al, 2018. Antioxidant efficiency of chitosan / graphene functionalized superparamagnetic iron oxide nanoparticles. *J. Mater. Sci. - Mater. Med.* <https://doi.org/10.1007/s10856-018-6163-0>.
- Hay RJ, Morris-jones R (2017) *Bacterial Infections*.
- Hossain, M.A., Elias, M., Sarker, D.R., Diba, Z.R., Mithun, J.M., Azad, M.A.K., Siddiquey, I.A., Rahman, M.M., Uddin, J., Uddin, M.N., 2018. Synthesis of Fe- or Ag-doped TiO₂-MWCNT nanocomposite thin films and their visible-light-induced catalysis of dye degradation and antibacterial activity. *Res. Chem. Intermed.* 44, 2667–2683.
- Huang, X., Qi, X., Boey, F., Zhang, H., 2012. Graphene-based composites. *Chem. Soc. Rev.* 41, 666–686. <https://doi.org/10.1039/c1cs15078b>.
- Hussain, S., Khakwani, N., Faiz, Y., Zulfiqar, S., Shafiq, Z., Faiz, F., Elhakem, A., Sami, R., Aljuraide, N.I., Farid, T., Aljabri, M.D., Rahman, M.M., 2022. Green production and interaction of carboxylated Cnts/ bio-genic ZnO composite for antibacterial activity. *Bioengineering* 9, 437.
- Jac, I., 2017. One pot hydrothermal synthesis characterizations of silver nanoparticles on reduced graphene oxide for its Enhance. *IOSR J. Appl. Chem. (IOSR-JAC)* 10 (64–69). <https://doi.org/10.9790/5736-1005016469>.
- Ji, H., Sun, H., Qu, X., 2016. Antibacterial applications of graphene-based nanomaterials: recent achievements and challenges. *Adv. Drug Deliv. Rev.* 105, 176–189. <https://doi.org/10.1016/j.addr.2016.04.009>.
- Khan, A.A.P., Khan, A., Rahman, M.M., Asiri, A.M., Oves, M., 2018. Chemical sensor development and antibacterial activities based on polyaniline/Gemini surfactants for environmental safety. *J. Polym. Environ.* 26, 1673–1684.
- Khan, M., Tahir, M.N., Adil, S.F., et al, 2015. Graphene based metal and metal oxide nanocomposites: synthesis, properties and their applications. *J. Mater. Chem. A* 3, 18753–18808. <https://doi.org/10.1039/c5ta02240a>.
- Leila, S., Athawale, A.A., 2014. Graphene oxide synthesized by using modified hummers approach. *Int. J. Renew. Energy Environ. Eng.* 02, 58–63.
- Lekshmi, G.S., Tamilselvi, R., Geethalakshmi, R., et al, 2022. Multifunctional oil-produced reduced graphene oxide – silver oxide composites with photocatalytic, antioxidant, and antibacterial activities. *J. Colloid Interface Sci.* 608, 294–305. <https://doi.org/10.1016/j.jcis.2021.08.048>.
- Menaa, F., Abdelghani, A., Menaa, B., 2015. Graphene nanomaterials as biocompatible and conductive scaffolds for stem cells: impact for tissue engineering and regenerative medicine. *J. Tissue Eng. Regen. Med.* 9, 1321–1338. <https://doi.org/10.1002/term.1910>.
- Menaa F, Fatemeh Y, Vashist SK, Iqbal H, Sharts ON, Menaa B (2021) Graphene, an Interesting Nanocarbon Allotrope for Biosensing Applications: Advances, Insights, and Prospects. *Biomed Eng Comput Biol.* 12:1179597220983821. doi: 10.1177/1179597220983821.
- Nanoparticles S, Bedlovı Z (2020) A Brief Overview on Antioxidant Activity. 1–24.
- Paquin, F., Rivnay, J., Salleo, A., et al, 2015. Multi-phase semicrystalline microstructures drive exciton dissociation in neat plastic semiconductors. *J. Mater. Chem. C* 3, 10715–10722. <https://doi.org/10.1039/b000000x>.
- Parsa, A., Salout, S.A., 2016. Investigation of the antioxidant activity of electrosynthesized polyaniline/reduced graphene oxide nanocomposite in a binary electrolyte system on ABTS and DPPH free radicals. *J. Electroanal. Chem.* 760, 113–118. <https://doi.org/10.1016/j.jelechem.2015.11.021>.

- Parthipan, P., Al-Dosary, M.A., Al-Ghamdi, A.A., Subramania, A., 2021. Eco-friendly synthesis of reduced graphene oxide as sustainable photocatalyst for removal of hazardous organic dyes. *J. King Saud Univ. - Sci.* 33., <https://doi.org/10.1016/j.jksus.2021.101438> 101438.
- Rajeswari, R., Prabu, H.G., 2018. Synthesis characterization, antimicrobial, antioxidant, and cytotoxic activities of ZnO nanorods on reduced graphene oxide. *J. Inorg. Organomet. Polym. Mater.* 28, 679–693. <https://doi.org/10.1007/s10904-017-0711-9>.
- Rakkappan R, Halliah GP (2020) I P re of. *Process Biochemistry*. doi: 10.1016/j.procbio.2020.03.010
- Ravichandran, K., Chidhambaram, N., Gobalakrishnan, S., 2016. Copper and Graphene activated ZnO nanopowders for enhanced photocatalytic and antibacterial activities. *J. Phys. Chem. Solid* 93, 82–90. <https://doi.org/10.1016/j.jpcs.2016.02.013>.
- Ray Chowdhuri, A., Tripathy, S., Chandra, S., et al, 2015. A ZnO decorated chitosan-graphene oxide nanocomposite shows significantly enhanced antimicrobial activity with ROS generation. *RSC Adv.* 5, 49420–49428. <https://doi.org/10.1039/c5ra05393e>.
- Rehana, D., Mahendiran, D., Kumar, R.S., Rahiman, A.K., 2017. Evaluation of antioxidant and anticancer activity of copper oxide nanoparticles synthesized using medicinally important plant extracts. *Biomed. Pharmacother.* 89, 1067–1077. <https://doi.org/10.1016/j.biopha.2017.02.101>.
- Rehman, F.U., Mahmood, R., Ben, A.M., et al, 2021. Physicochemical, photocatalytic, antibacterial, and antioxidant screening of *Bergenia Ciliata* mediated nickel oxide nanoparticles. *Crystal* 11, 1137. <https://doi.org/10.3390/cryst11091137>.
- Sen, S., 2010. Free radicals, antioxidants, diseases and phytomedicines : current status and future prospect. *Int. J. Pharma. Sci. Rev. Res.* 3, 91–100.
- Shadmehri, A.A., Namvar, F., Miri, H., Yaghmaei, P., 2019. Assessment of antioxidant and antibacterial activities of Zinc Oxide nanoparticles. *Graph. Graph. Decorated Zinc Oxide Nanopart.* 10, 350–358.
- Shah, A., Tauseef, I., Arfat, M., et al, 2023. Histopathological and hematological investigations of mice model inoculated with nickel oxide nanoparticles and bacterial pathogens : in-vitro and in-vivo antibacterial studies. *J. King Saud Univ. - Sci.* 35., <https://doi.org/10.1016/j.jksus.2022.102456> 102456.
- Shoukat, S., Rehman, W., Haq, S., et al, 2019. Synthesis and characterization of zinc stannate nanostructures for the adsorption of chromium (VI) ions and photo-degradation of rhodamine 6G. *Mater. Res. Express* 6., <https://doi.org/10.1088/2053-1591/ab473c> 115052.
- Singh, V., Joung, D., Zhai, L., et al, 2011. Graphene based materials: past, present and future. *Prog. Mater Sci.* 56, 1178–1271. <https://doi.org/10.1016/j.pmatsci.2011.03.003>.
- Singh, R.K., Kumar, R., Singh, D.P., 2016. Graphene oxide: Strategies for synthesis, reduction and frontier applications. *RSC Adv.* 6, 64993–65011. <https://doi.org/10.1039/c6ra07626b>.
- Sorbiun, M., Shayegan, E., Ali, M., 2018. Green synthesis of Zinc Oxide and Copper Oxide nanoparticles using aqueous extract of oak fruit hull (Jaft) and comparing their photocatalytic degradation of basic Violet 3. *Int. J. Environ. Res.* 12, 29–37. <https://doi.org/10.1007/s41742-018-0064-4>.
- Subhan, M.A., Saha, P.C., Rahman, M.M., Ahmed, J., Asiri, A.M., Al-Mamun, M., 2018. Fabrication of a 2,4-dinitrophenol sensor based on Fe₃O₄@Ag@Ni nanomaterials and studies of their antibacterial properties. *New J. Chem.* 42, 872–881.
- Subhan, M.A., Jhuma, S.S., Saha, P.C., Alam, M.M., Asiri, A.M., Al-Mamun, M., Attia, S.A., Emon, T.H., Azad, A.K., Rahman, M. M., 2019. Efficient selective 4-aminophenol sensing and antibacterial activity of ternary Ag₂O₃-SnO₂-Cr₂O₃ nanoparticles. *New J. Chem.* 43, 10352–10365.
- Subhan, M.A., Rifat, T.P., Saha, P.C., Alam, M.M., Asiri, A.M., Rahman, M.M., Akter, S., Raihan, T., Azad, A.K., Uddin, J., 2020. Enhanced visible light mediated photocatalysis, antibacterial functions and fabrication of 3-Chlorophenol sensor based on ternary Ag₂O.SrO.CaO. *RSC Adv.* 10, 11274–11291.
- Taghioskoui, M., 2009. Trends in graphene research. *Mater. Today* 12, 34–37. [https://doi.org/10.1016/S1369-7021\(09\)70274-3](https://doi.org/10.1016/S1369-7021(09)70274-3).
- Uddin, M.N., Islam, M.S., Mazumder, M.M.R., Hossain, M.A., Elias, M., Siddiquey, I.A., Susan, M.A.B.H., Saha, D.K., Rahman, M. M., Asiri, A.M., Hayami, S., 2015. Photocatalytic and antibacterial activity of B/N/Ag co-doped CNT–TiO₂ composite films. *J. Incl. Phenom. Macrocycl. Chem.* 82, 229–234.
- Ur Rehman, M., Rehman, W., Waseem, M., et al, 2018. Adsorption of Pb²⁺ ions on novel ternary nanocomposite of tin, iron and titania. *Mater. Res. Express*. <https://doi.org/10.1088/2053-1591/aaabd8>.
- Xie, Y.Y., Hu, X.H., Zhang, Y.W., et al, 2020. Development and antibacterial activities of bacterial cellulose/graphene oxide-CuO nanocomposite films. *Carbohydr. Polym.* 229., <https://doi.org/10.1016/j.carbpol.2019.115456> 115456.
- Yoo, M.J., Park, H.B., 2019. Effect of hydrogen peroxide on properties of graphene oxide in Hummers method. *Carbon* 141, 515–522. <https://doi.org/10.1016/j.carbon.2018.10.009>.